

Simulating PFAS adsorption kinetics, adsorption isotherms, and
nonideal transport in saturated soil with tempered one-sided stable
density (TOSD) based models

Dongbao Zhou et al.

Deposited 2023-09-27

Citation of published version:

Zhou, D., Brusseau, M. L., Zhang, Y., Li, S., Wei, W., Sun, H., & Zheng, C. (2021).
Simulating PFAS adsorption kinetics, adsorption isotherms, and nonideal
transport in saturated soil with tempered one-sided stable density (TOSD) based
models. In *Journal of Hazardous Materials* (Vol. 411, p. 125169). Elsevier BV.
<https://doi.org/10.1016/j.jhazmat.2021.125169>



Published in final edited form as:

J Hazard Mater. 2021 June 05; 411: 125169. doi:10.1016/j.jhazmat.2021.125169.

Simulating PFAS adsorption kinetics, adsorption isotherms, and nonideal transport in saturated soil with tempered one-sided stable density (TOSD) based models

Dongbao Zhou^a, Mark L. Brusseau^b, Yong Zhang^{c,*}, Shiyin Li^d, Wei Wei^d, HongGuang Sun^a, Chunmiao Zheng^e

^aCollege of Mechanics and Materials, Hohai University, Nanjing, Jiangsu 210098, China

^bSoil, Water, and Environmental Science Department, University of Arizona, Tucson, AZ 85721, USA

^cDepartment of Geological Sciences, University of Alabama, Tuscaloosa, AL 35487, USA

^dSchool of Environment, Nanjing Normal University, Nanjing, Jiangsu 210023, China

^eSchool of Environmental Science & Engineering, Southern University of Science and Technology, Shenzhen 518055, Guangdong, China

Abstract

Reliable quantification of per- and polyfluoroalkyl substances (PFAS) adsorption and mobility in geomeedia provides critical information (i.e., evaluation and prediction) for risk characterization and mitigation strategy development. Given the limited PFAS data available and various competing theories for modeling pollutant kinetics, it is indispensable to better understand and quantify the adsorption and transport of PFAS in geomeedia using generalized models built upon a consistent physical theory. This study proposed a universal physical law (called the tempered stable law) in PFAS adsorption/transport by interpreting PFAS adsorption kinetics and nonideal transport as a nonequilibrium process dominated by adsorption/desorption with multiple rates following the tempered one-sided stable density (TOSD) distribution. This universal TOSD function led to novel TOSD-based models which were then tested by successfully simulating PFAS adsorption kinetics, adsorption isotherms, and nonideal transport data reported in the literature. Model comparisons and extensions were also discussed to further check the feasibility of the TOSD models and their adaptability to capture PFAS transport in more complex geomeedia at all scales.

*Corresponding author: yzhang264@ua.edu.

[†] Author statement

In this manuscript, Dongbao Zhou is the first author who modeled the data and prepared most part of the original draft significantly rewritten by Yong Zhang. Mark Brusseau and Chunmiao Zheng received funding for this research. Mark Brusseau, Yong Zhang, Wei Wei, Shiyin Li, and HongGuang Sun contributed to the interpretation of the results and revision of the manuscript for intellectual content and approved the final version of the manuscript. Yong Zhang proposed the research idea and was the main advisor for this work.

Declaration of Competing Interest

The authors declare that they have no known competing financial interests or personal relationships that could have appeared to influence the work reported in this paper.

Appendix A. Supplementary data

Supplementary material related to this work is attached.

Keywords

PFAS; adsorption kinetics and isotherm; transport; tempered one-sided stable density

1. INTRODUCTION

Per- and polyfluoroalkyl substances (PFAS) are synthetic, organic chemicals that were or are present in numerous consumer products, such as nonstick pans, food packaging, and waterproof clothing, and used for industrial purposes due to their thermal stability and hydrophobic properties (Buck et al., 2011; USEPA, 2019). Owing mainly to industrial release and firefighting foam, PFAS are emerging contaminants in soil and/or groundwater that have been found present worldwide. They pose risks to the health of both freshwater ecosystems and human beings due to their non-degradability and toxicity (e.g., Jian et al., 2017; Rappazzo et al., 2017). Many efforts (briefly reviewed below) have been made to characterize PFAS adsorption and/or mobility in soil, including 1) adsorption isotherms, 2) adsorption kinetics, and 3) transport, but a comprehensive and consistent description of PFAS dynamics in the subsurface is still needed for efficient management (Brusseau, 2020). This study aims to quantify PFAS adsorption kinetics, adsorption isotherms, and nonideal transport in saturated soils using generalized models built upon a consistent physical theory, to understand and better quantify the fate and transport of PFAS in saturated soil.

First, PFAS adsorption isotherms relate the amount of adsorbate sorbed to the adsorbent (which is soil in this study) to the aqueous concentration of PFAS at a given temperature. Various (up to 15) isotherm models have been developed to describe equilibrium adsorption for chemicals under various physical, chemical, and biological conditions (Limousin et al., 2007; Qiu et al., 2009). Batch experiments show that PFAS adsorption isotherms exhibit a linear (e.g., Milinovic et al., 2015; Miao et al., 2017) or power-law relation (e.g., Higgins and Luthy, 2006; Zhang et al., 2013; Chen et al., 2016; Liu et al., 2018) between the adsorbed and aqueous concentrations at equilibrium. Different adsorption isotherm models, including the Langmuir and Freundlich models, were applied to capture PFAS adsorption isotherms; see the extensive review by Foo and Hamed (2010). Various expressions of PFAS adsorption isotherms may lead to inconsistent physical explanations of model parameters (Foo and Hameed, 2010). A general model with appropriate physical basis, therefore, is needed for capturing the various PFAS adsorption isotherms identified above, which is the first goal of this study.

Second, PFAS adsorption kinetics involve the time evolution of thermodynamic quantities under non-equilibrium conditions. Prior laboratory experiments have revealed that PFAS adsorption by soil is rate limited (Zhang et al., 2011; Chen et al., 2013; Zhang et al., 2013; Li et al., 2019). The kinetics of PFAS adsorption by soil and other geomedias can be regarded as a random process continuously competing with desorption. Various sorption-reaction models have been developed to describe the kinetics of adsorption, such as the pseudo-first and pseudo-second order equations assuming the rate of surface reaction as the rate-limiting step (Ho et al., 2000; Plazinski et al., 2009). The adsorption rate of PFAS for natural media such as soil is not limited to the constant rate assumed by the pseudo-first/second order

equations but may be a random variable with a distribution. For example, the transport of PFOS in soil exhibited nonideal behavior that could only be accurately simulated with use of a multi-rate mass-transfer model (Brusseau et al., 2019). Multi-rate models usually require multiple parameters. To check whether this challenge can be solved, this study will propose and test a general model, with few parameters, for reliably quantifying adsorption kinetics for various PFAS and multiple soils.

Third, PFAS transport in heterogeneous, saturated soil may be influenced by rate-limited and nonlinear adsorption/desorption, as well as diffusive mass transfer between advective flow regions and relatively immobile domains in physically heterogeneous media. The impact of these phenomenon can cause transport to be nonideal, wherein for example breakthrough curves (BTCs) exhibit early breakthrough and/or extended tailing. Laboratory experiments conducted by Brusseau et al. (2019a, 2019b) illustrated nonideal transport behavior of PFOA in soil. The complex transport of PFAS can be quantified by various models. For example, Brusseau et al. (2019a) employed a continuous-distribution, multi-rate (CDMR) model (see Eq. (S1) in Supplementary Information (SI)) by assuming multi-rate adsorption kinetics. Parsimonious, stochastic methods have been applied to model solute retention, including the well-known continuous-time random walk (CTRW) framework (Berkowitz et al., 2006), the multi-rate mass transfer (MRMT) model (Haggerty et al., 2000), and the relatively new fractional-derivative equations (FDEs) (Meerschaert et al., 2008). To keep consistent with the models developed for PFAS adsorption, this study will adopt the FDE (which contains less parameters than the CTRW and MRMT models, as demonstrated by Lu et al. (2018)) to model PFAS transport in saturated soil and evaluate the impact of adsorption on PFAS transport.

To model PFAS adsorption isotherms, kinetics, and transport, the study is organized as follows. Section 2 reviews PFAS adsorption isotherm experiments documented in the literature, and then develops and checks the general physical model using the tempered one-sided stable density (TOSD) function for capturing PFAS adsorption under equilibrium in soil. Section 3 reviews PFAS adsorption kinetics studies, and then proposes and tests the TOSD-based rate equation to model PFAS concentration evolution in the adsorption/desorption process. Section 4 adopts the FDE, which is built upon the TOSD-based memory function, to model nonideal transport of PFAS in soil columns. Section 5 discusses the common processes and characteristics of PFAS adsorption and mobility, evaluates the parameters in the TOSD-based models, and compares the new and previous models. Section 6 summarizes the main conclusions.

2. TOSD-BASED ISOTHERM MODEL FOR PFAS ADSORPTION ISOTHERMS

2.1 Literature Review: PFAS Adsorption Isotherm Experiments

Dataset 1 from Li et al. (2019)—Li et al. (2019) measured adsorption isotherms for five PFAS (listed in Table 1) adsorbed to surficial soils collected from China. Batch adsorption experiments were performed with different initial PFAS concentrations. The observed adsorption isotherm data for soil type 6 are shown by symbols in Fig. 1. Li et

al. (2019) found that the observed adsorption isotherms can be well represented by the Freundlich isotherm model (Fig. 1):

$$C_S = k_F C_W^n, \quad (1)$$

where C_S (nmol/kg) is the equilibrium concentration of PFAS in solid phase, C_W (nM) is the aqueous-phase equilibrium concentration of PFAS, k_F ((nmol/kg)/(nM)ⁿ) is the Freundlich distribution coefficient, and n (dimensionless) is the Freundlich exponent. This dataset and model (1) will be used to check the applicability of the adsorption isotherm formula developed below.

Dataset 2 from Cao et al. (2017)—Cao et al. (2017) conducted batch adsorption experiments to explore PFOS adsorption by both molecularly imprinted polymers (MIPs) and non-imprinted polymers (NIPs) (see symbols in Fig. 2). These data were used in the current study as a different type of medium to obtain a broader test. Different from the dataset 1 reviewed above, Cao et al. (2017) found that the Langmuir model (2) fits the data better than the Freundlich model (1):

$$C_S = \frac{C_m}{\frac{1}{k_L} + C_W} C_W, \quad (2)$$

where C_m (mg/g) is the theoretical maximum capacity, and k_L (L/mg) is the Langmuir constant. The best-fit solutions using both model (1) and model (2) are plotted in Fig. 2 and will be compared with the solution of the new isotherm model proposed in the next section.

2.2 Development of the TOSD-Isotherm Model for PFAS Adsorption Isotherms

The observed PFAS adsorption isotherms (Figs. 1 and 2) exhibit either a pure power-law or truncated power-law behavior (therefore neither model (1) nor (2) can capture all the curves), requiring a general probability density function (PDF) to describe the variable adsorption rate. Hence, we adopt the tempered fractional derivative proposed by Meerschaert et al. (2008) to quantify PFAS adsorption at equilibrium:

$$e^{-\lambda C_W} \frac{\partial^\alpha (e^{\lambda C_W} C_S)}{\partial C_W^\alpha} = k, \quad (3)$$

where λ (kg/nmol) is the truncation parameter (used to truncate the power-law function and control the transition from the power-law relation to the exponential relation), and α ($0 < \alpha < 1$) (dimensionless) is the index of the Caputo fractional derivative defined as (Miller and Ross, 1993):

$$\frac{\partial^\alpha \varphi}{\partial t^\alpha} = \frac{1}{\Gamma(m-\alpha)} \int_0^t (t-\tau)^{m-\alpha-1} \varphi^m(\tau) d\tau, \quad (4)$$

where m (dimensionless) is the minimum integer no less than α (here $m=1$), and $\Gamma(\cdot)$ is the gamma function. Eq. (3) can be re-written as:

$$e^{-\lambda c_w} \frac{1}{\Gamma(1-\alpha)} \int_0^{c_w} (c_w - \tau)^{-\alpha} e^{\lambda c_w c_s d \tau} \frac{1}{k} , \quad (5)$$

where the left-hand side denotes the tempered Caputo fractional derivative (Meerschaert et al., 2008). Taking Laplace transform of (5) and then the inverse Laplace transform, we derive the first TOSD-based model (TOSD-isotherm model) in this study:

$$c_s = k c_w^\alpha E_{1, \alpha+1}^\alpha(-\lambda c_w) , \quad (6)$$

where the symbol $E_{1, \alpha+1}^\alpha$ denotes the generalized Mittag-Leffler function

$E_{1, \alpha+1}^\alpha(x) = \sum_{n=0}^{\infty} \frac{1}{(n+\alpha)\Gamma(\alpha)} \frac{x^n}{n!}$. When $\lambda = 0$, Eq. (6) reduces to a pure power-law form of isotherm model:

$$c_s = \frac{k c_w^\alpha}{\Gamma(\alpha+1)} . \quad (7)$$

The simplified version (7) is similar to the Freundlich isotherm model (1), showing that the TOSD-isotherm model (6) is more general than model (1), which will be checked below. By adjusting the truncation parameter λ and the index α , model (6) can capture a broad range of relationships between c_s and c_w , including the power-law function, the exponential function, and any transition between them.

2.3 TOSD-Isotherm Model Applications

Dataset 1 from Li et al. (2019)—Parameters of the TOSD-isotherm model (6) (listed in Table 1) are fitted by the observed adsorption isotherms (Fig. 1) using the least-square method (Zhou et al., 2011). Model solutions match the adsorption isotherms for all PFAS, which exhibit power-law behaviors (Fig. 1b). The best-fit index α decreases with an increase of the PFAS chain length (Table 1), which is consistent with the fact that PFAS with larger chain lengths are more favorable to soil adsorption (e.g., Higgins and Luthy, 2006). Notably, PFPeA and PFBS have the same chain length, but the index α for PFBS is smaller than that for PFPeA. This discrepancy might be due to the presence of sulfonate groups in PFBS (C₄HF₉O₃S), which enhances the adsorption of PFBS by soil.

Dataset 2 from Cao et al. (2017)—The TOSD-isotherm model (6) can also fit the observed adsorption isotherms of PFOS onto NIPs and MIPs, with a truncated power-law concentration curve (Fig. 2) (with the best-fit parameters listed in Table 2). A detailed model comparison will be discussed in section 5.3.

3. TOSD-KINETIC MODEL FOR PFAS ADSORPTION KINETICS

3.1 Literature Review: PFAS Adsorption Kinetics Experiments

Dataset 3 from Li et al. (2019)—Li et al. (2019) monitored PFOA adsorption kinetics in soil (Fig. 3). They found that the adsorption kinetics can be well fitted by the biexponential adsorption model:

$$F_W = F_0 + F_1 e^{-k_1^* t} + F_2 e^{-k_2^* t}, \quad (8)$$

where F_W (dimensionless) is the fraction of aqueous phase PFAS at time t , F_0 is the fraction of aqueous phase PFAS at equilibrium; and F_1 and F_2 represent the fraction of PFAS adsorbed onto soil at the independent adsorption rate k_1^* (h^{-1}) and k_2^* , respectively. The biexponential adsorption model (8) will be compared with the new model proposed in section 3.2.

Dataset 4 from Wei et al. (2017)—Wei et al. (2017) conducted PFOS adsorption kinetics experiments using various soils. Six soil samples were collected as adsorbents from six provinces/cities in China, including Jiangxi (JX), Guangdong (GD), Guangxi (GX), Heilongjiang (HLJ), Jiangsu (JS), and Chongqing (CQ). The measured PFOS kinetic concentrations (Fig. 4) show that the adsorbed concentration at equilibrium follows the order (from high to low) of GD>HLJ>JX>CQ>GX>JS.

3.2 Development of the TOSD-Kinetic Model for PFAS Adsorption Kinetics

The Lagergren rate equation may have been the first developed rate equation and is the most widely used method for quantifying adsorption kinetics in liquid-solid systems (Lagergren, 1898):

$$\frac{dS_t}{dt} = k_1(S_e - S_t), \quad (9)$$

where k_1 is the first-order reaction rate, S_t is the adsorbed concentration of PFAS on the solid phase at time t , and S_e is the adsorbed concentration of PFAS on the solid phase at equilibrium. The analytical solution of the Lagergren equation (9) is:

$$S_t = k_1 e^{-k_1 t} * S_e + e^{-k_1 t} S_0, \quad (10)$$

where the symbol “*” denotes convolution, $k_1 e^{-k_1 t}$ is the convolution kernel which is similar to the memory function used to define the exponential distribution for waiting times for solute particles trapped by immobile domains (Schumer et al., 2003), and S_0 is the initial concentration for the adsorbed phase. Assuming $S_0=0$, solution (10) reduces to:

$$S_t = (1 - e^{-k_1 t}) S_e, \quad (11)$$

showing that the rate for S_t to approach S_e depends on k_1 under an initially clean condition for the adsorbed phase.

The analytical solutions (10) and (11) exhibit singular, exponential adsorption. However, as reported for kinetic adsorption experiments (see the ones reviewed above), the single reaction rate in the exponential adsorption kinetic model is not sufficient to capture complex adsorption of PFAS in nonideal, saturated soils which can exhibit multiple adsorption rates. A general multi-rate model capturing PFAS adsorption in soil takes the form:

$$S_t = \sum_j^N \beta_j S_t^j \quad (12)$$

$$\frac{dS_t^j}{dt} = k_j(S_e - S_t^j), \quad j = 1, 2, 3, \dots, N \quad (13)$$

Eqs. (12) and (13) account for the multi-rate adsorption of PFAS in soil, where adsorption is divided into N sites with different rates. Assuming the initially clean condition $S_0=0$, the analytical solution of Eqs. (12) and (13) is:

$$S_t = (1 - \sum_j^N \beta_j e^{-k_j t}) S_e, \quad (14)$$

which leads to $S_t \rightarrow S_e$ when $t \rightarrow \infty$. For the simplified two-site case ($N=2$), Eq. (14) reduces to a biexponential adsorption model used for PFAS adsorption kinetics (Higgins and Luthy, 2006; Li et al., 2019), such as Eq. (8) reviewed above.

This study assumes that the rate of PFAS adsorption to the soil surface has a distribution following the TOSD function, which is functionally equivalent to the following truncated power-law memory function $f(t)$ (Meerschaert et al., 2008)

$$f(t) = \int_t^\infty e^{-\lambda \tau} \frac{\alpha \tau^{-\alpha-1}}{\Gamma(1-\alpha)} d\tau \quad (15)$$

describing the PFAS adsorption kinetics:

$$S_t = f(t) * S_e. \quad (16)$$

Eq. (16) is the 2nd TOSD-based model proposed by this study (named the ‘‘TOSD-kinetics’’ model herein), for quantifying PFAS adsorption kinetics. The analytical solution for the concentration of PFAS in the solid phase for the TOSD-kinetics model (16) is:

$$S_t = S_e t^{1-\alpha} E_{1,2-\alpha}^{-\alpha}(-\lambda t) - S_e \lambda^\alpha t. \quad (17)$$

Assuming that 1) the concentration of the initially injected aqueous-phase PFAS is C_0 , and 2) the aqueous equilibrium concentration is C_e , the corresponding concentration of PFAS remaining in the aqueous phase at time t can be expressed by:

$$C_t = C_0 - (C_0 - C_e) [t^{1-\alpha} E_{1,2-\alpha}^{-\alpha}(-\lambda t) - \lambda^\alpha t]. \quad (18)$$

This formula will also be applied to derive the model for PFAS transport in soil in section 4.

3.3 TOSD-Kinetic Model Applications

Dataset 3 from Li et al. (2019)—The TOSD-kinetic model solution (18) generally matches the observed adsorption kinetics for all five types of PFAS observed by Li et al. (2019) (Fig. 3). The measured aqueous concentration profile for each of the PFAS (Fig. 3) exhibits an apparent change in adsorption kinetics (i.e., with a transition of the rate of decrease of the aqueous mass) after 25~40 h, which was also reported by Li et al. (2019). This transition can be captured by the TOSD-kinetic model (18), whose aqueous mass declines with a transition rate controlled by the truncation parameter λ . The best-fit λ values for all PFAS in Fig. 3 are larger than 0.1 (h^{-1}) (Table 3), implying a transition from power-law adsorption to exponential adsorption, which is analogous to the phenomenon that solute transport transfers from anomalous to normal diffusion in natural media (Sun et al., 2014).

The fraction of PFAS finally remaining in the aqueous phase (i.e., the equilibrium concentration C_e) decreases with increasing PFAS chain length, which is consistent with the result of adsorption isotherms in Li et al. (2019). This is because the longer the perfluorinated acid chain, generally the greater the adsorption of PFAS on soil. Both the best-fit index α and the truncation parameter λ in the TOSD-kinetic model (18) slightly fluctuate for different PFAS (Table 3).

Dataset 4 from Wei et al. (2017)—The TOSD-kinetic model (18) can capture the overall pattern of the adsorption kinetics of PFOS in all six soils observed by Wei et al. (2017) (Fig. 4), with the best-fit parameters listed in Table 4. The best-fit index α in model (18) for the six soils varies and follows the order of JX>GX>HLJ>CQ>GD>JS, implying the possible effect of soil properties on PFOS adsorption. Electrostatic interaction, hydrophobic interaction, and hydrogen bonding in soil (note that these properties can change significantly between different soils) were found by Wei et al. (2017) to be the main factors affecting the adsorption kinetics of PFOS, whose impact may be described by the parameters α and λ .

4. TOSD-TRANSPORT MODEL FOR PFAS TRANSPORT IN SOIL

4.1 Literature Review: PFAS Column Transport Experiments

Dataset 5 from Brusseau et al. (2019a): Transport of PFOS in soil—Brusseau et al. (2019a) conducted miscible-displacement transport experiments to explore the transport of PFOS in two soils. The columns were 15~20 cm long with an inner diameter of 2~2.5 cm and filled with air-dried soils: Eustis and Vinton, respectively. The Eustis soil is composed primarily of quartz, while the Vinton soil contains silica, feldspar, amphibole, and clay minerals. Each column (oriented vertically) was first saturated with electrolyte solution from bottom to top, followed by a pulse injection of 10 mg/L PFOS with a constant flow rate of 1 mL/min. The measured PFOS BTCs from Eustis and Vinton show apparent late-time tailing behaviors (shown by symbols in Fig. 5). This late-time tailing is similar to the power-law concentration profiles observed in the adsorption experiments discussed above. Brusseau et

al. (2019a) found that the CDMR model (Eq. (S1) in SI) can capture the observed PFOS concentration profile.

Dataset 6 from Lv et al. (2018): Transport of PFOA in quartz sand and limestone porous media

—In the column transport experiments reported by Lv et al. (2018), the column length and inner diameter are 16.7 cm and 2.5 cm, respectively. The columns were packed with either artificially treated quartz sand (geochemically reactive constituents removed) or crushed limestone. The observed BTCs of PFOA transport in the limestone column and the quartz sand column are plotted in Figs. 6a and 6b, respectively. Lv et al. (2018) applied the following two-site model to capture the observed PFOA concentration profile (shown by the dashed line in Fig. 6):

$$\frac{\partial C}{\partial t} + \frac{\rho}{\theta} \frac{\partial S_1}{\partial t} + \frac{\rho}{\theta} \frac{\partial S_2}{\partial t} = -v \frac{\partial C}{\partial x} + D \frac{\partial^2 C}{\partial x^2} \quad (19a)$$

$$\frac{\rho}{\theta} \frac{\partial S_1}{\partial t} = k_1 C \quad (19b)$$

$$\frac{\rho}{\theta} \frac{\partial S_2}{\partial t} = k_2 C - \frac{\rho}{\theta} k_3 S_2 \quad (19c)$$

where C (g/cm^3) is the concentration of PFOA in the aqueous phase; S_1 and S_2 (g/g) are the solid-phase PFOA concentrations associated with the adsorption sites 1 and 2, respectively; k_1 and k_2 (h^{-1}) are the first-order adsorption coefficients of sites 1 and 2, respectively; and k_3 (h^{-1}) is the desorption coefficient of site 2. Model (19) is a mixed equilibrium-kinetic model.

Dataset 7 from Guelfo et al. (2020): Transport of PFOA and PFOS in four different soils

—Guelfo et al. (2020) conducted column experiments to investigate PFAA transport in soils/sand with different organic carbon fractions (f_{oc}): Soil A (loamy sand with 81% of sand, 10% of silt, and 9% of clay, and $f_{oc}=0.017$), Soil B (loam with 31% of sand, 42% of silt, and 25% of clay, and $f_{oc}=0.045$), Soil C (loamy sand with 80% of sand, 12% of silt, and 8% of clay, and $f_{oc}=0.0017$), and Sand (100% of medium silica sand with $f_{oc}=0$ and the size of 0.297~0.420 mm). The uniformly packed soil or sand columns were 5 cm long with an inner diameter of 2.5 cm. In each column experiment, PFAAs were injected into the saturated medium until the relative concentration (C/C_0) approached ~1 for all PFAAs. The BTCs of PFOSs and PFOAs and in Soils A~C and Sand (shown by symbols in Fig. 7 and Fig. S3, respectively) were observed by Guelfo et al. (2020) to be related to compound chain length and soil f_{oc} (which are the two primary factors affecting PFAA adsorption in batch studies). Our inspection of the figures reveals the presence of elution tailing behavior in their observed BTCs. For example, the PFOS BTCs (Fig. 7) exhibited a more extensive elution tail than that for PFOA BTCs (Fig. S3). The standard two-site model (19) containing one instantaneous adsorption site and one first-order kinetic adsorption site was applied by Guelfo et al. (2020) to simulate the PFAA BTCs. Results show that this simplified model underestimated the BTCs with a late-time tail (see **Figures 1, S4, and S10** in Guelfo et

al. (2020)), implying rate-limited adsorption in PFAS transport. We will check whether the TOSD-transport model shown below can improve the model fitting.

4.2 TOSD-Transport Model for PFAS Transport in Soil

Previous studies show that two-site models and mobile-immobile models (see Eq. (S4) in SI) are inadequate for describing nonideal solute transport with heavy-tailed (i.e., power-law) BTCs, while the heavy-tailed BTCs are widely observed in long term flushing experiments in porous media (Brusseau, 1995; Bromly et al., 2004). The mass exchange rate (for solute retention) between the mobile region and the relatively immobile regions, such as the adsorption/desorption rate between the aqueous phase PFAS and the adsorbed phase, may show a power-law PDF (see discussion in section 3). Here we assume that the overall mass exchange rate of PFAS follows the TOSD distribution. This assumption leads to the governing equation (see Meerschaert et al. (2008) for derivation):

$$\frac{\partial C_a}{\partial t} + \beta \frac{\partial C_a}{\partial t} * g(t) = -v \frac{\partial C_a}{dx} + D \frac{\partial^2 C_a}{\partial x^2} \quad (20)$$

where the memory function $g(t)$ takes the form of (15). Hence, we obtain the TOSD-transport model for PFAS transport (the 3rd TOSD-based model in this study):

$$\frac{\partial C_a}{\partial t} + \beta e^{-\lambda t} \frac{\partial^\alpha (e^{\lambda t} C_a)}{\partial t^\alpha} - \beta \lambda^\alpha C_a = -v \frac{\partial C_a}{dx} + D \frac{\partial^2 C_a}{\partial x^2}, \quad (21)$$

which is the same as the fractional-derivative model proposed by Meerschaert et al. (2008) to capture transient anomalous diffusion due to diffusive mass transfer between advective flow regions and immobile domains. Eq. (21) is a general model for capturing the combined effects of adsorption/desorption and diffusive mass transfer on PFAS transport in soil. Notably, the tempered stable density is infinitely divisible (Baeumer et al., 2009), meaning that the TOSD-based physical models applicable at the laboratory scale are also mathematically valid at a larger scale.

Both the TOSD-transport model (21) and the two-site model (19) are solved here using an implicit finite difference method. Stability and convergence of the finite difference method for the TOSD-transport and MIM models can be found in Meerschaert et al. (2004). The solutions of models (21) and (19) are then fitted by the observed BTCs using the least square minimization method with the Levenberg-Marquardt algorithm (Zhou et al., 2011).

We also use a 90% confidence interval to describe the uncertainty of the time index (α) and fractional capacity coefficient (β). The margin of error is defined as (Altman et al., 2013): $Z = 1.645 \frac{\sigma}{\sqrt{n}}$, where Z is the error margin, n is the number of the samples for α or β , and σ is the standard deviation of the sampling data. The result of sensitivity analysis of parameters in the TOSD-transport model (21) is also shown in section S3 in the SI.

4.3 TOSD-Transport Model Applications

Dataset 5 from Brusseau et al. (2019a): Transport of PFOS in soil—The best-fit parameters are listed in Table 5. The TOSD-transport model (21) simulation provides a good match with the observed PFOS BTCs for both Eustis and Vinton soil (Fig. 5). The best-fit time index α values in model (21) are 0.85 and 0.95 for PFOS transport in Eustis and Vinton soil, respectively, showing the effect of soil properties on PFAS transport for the same PFAS. The best-fit truncation parameter λ is 0.046 and 0.047 h⁻¹ for Eustis and Vinton soil, respectively, which are relatively small, implying that the transport of PFOS in the soil column was affected by rate-limited mass exchange.

Dataset 6 from Lv et al. (2018): Transport of PFOA in quartz sand and limestone porous media—The best-fit parameters are listed in Table 6. The TOSD-transport model (21) provides a good simulation of the observed PFOA BTCs in the quartz sand and limestone columns, where the late-time BTC tail is either apparently heavy (i.e., as long as a power-law function) (Fig. 6a) or light (i.e., as short as an exponential function) (Fig. 6b). The best-fitted velocity v values in model (21) are 12.2 and 10.6 cm/h for the quartz sand and limestone columns, respectively, which are equal or close to the velocity (12.2 cm/h) reported by Lv et al. (2018). The time index α in model (21) is 0.94 (close to 1) for quartz sand (Table 6), capturing the short BTC tail shown in Fig. 6d. The short tail of the PFOA BTC might be due to the weak adsorption of PFOA on the treated quartz. Conversely, the time index α in model (21) is 0.25 for PFOA transport in the limestone column, and the apparently extensive late-time tail in the BTC can be observed in Fig. 6c, implying the strong effect of adsorption on the transport of PFOA in the crushed-limestone, probably due to the relatively larger specific surface area and less negative zeta-potential of the limestone compared to that of the quartz sand.

Dataset 7 from Guelfo et al. (2020): Transport of PFOA and PFOS in soils/sand with different f_{oc} —The TOSD-transport model (21) captures the BTCs for both PFOS and PFOA in Soils A-C and Sand (Fig. 7 and Fig. S3), with the best-fit parameters listed in Table 7 and Table S3, respectively. The fitted index α for PFOA is relatively larger than that for PFOS, likely due to the smaller adsorption capacity of PFOA than PFOS reported by Guelfo et al. (2020). The best-fit α for either PFOA or PFOS transport in Soil B (with the largest f_{oc}) is smaller than the other three media, showing stronger adsorption with a higher organic carbon fraction. The transport behavior of PFOA in Sand (Figs. S3d and S3h) is similar to that of PFOA transport in quartz sand reported by Lv et al. (2018) (Figs. 6b and 6d), both with a short tail and fitted by a relatively large α . However, an apparent extensive late-time BTC tail was observed for PFOS transport in Sand (Figs. 7d and 7h), consistent with stronger adsorption of PFOS than PFOA by the silica sand.

5. DISCUSSION

5.1 PFAS Adsorption and Transport with a TOSD Distributed Rate

PFAS adsorption by soil exhibits multiple rates due to the intrinsic geochemical heterogeneity of natural soil constituents. The adsorption rate of PFAS may depend on multiple soil properties, including specific surface area, organic carbon content and

composition, metal oxide content (Fe, Mn, Al), clay mineralogy, and intraparticle pore structure. For example, PFAS can be adsorbed by soil or sediment via interaction of the hydrophobic fluorinated carbon tail with the organic carbon fraction of the soil, and electrostatic interactions of the polar head group with the charged clay or metal-oxide fractions (e.g., Higgins and Luthy, 2006; Kucharzyk et al., 2017). Therefore, various chemical properties can affect PFAS adsorption rates in soil, expanding the distribution of PFAS adsorption rates and resulting in extended tailing of PFAS concentration profiles for PFAS adsorption kinetics and transport.

Transport of PFAS in soil is also a multi-process phenomenon since it involves both adsorption kinetics and diffusive mass transfer, and adsorption kinetics due to geochemical heterogeneity of soil may play a dominant role in nonideal transport of PFAS in packed-soil column experiments (Brusseau et al., 2019a). This can be seen in Brusseau et al. (2019a) who compared the transport of conservative tracer and PFAS through soil columns. In addition, the PFAS adsorption batch experiments discussed above revealed that adsorption/desorption equilibrium was achieved within 5 to 24 hours, longer than the typical column transport time scale (<2 hours in the literature reviewed above), and resulting in various late-time tails in PFAS BTCs. Hence, the late-time tailing for PFAS transport in soil/sand columns is mainly driven by the multi-rate adsorption/desorption in geochemically heterogeneous systems, while the late-time tailing for conservative tracer transport in soil/sand columns documented in hydrologic literature (Haggerty et al., 2000; Zhang et al., 2009) is mainly driven by diffusive mass transfer in physically heterogeneous systems.

Each specific rate of adsorption results in one exponential function describing the concentration evolution in PFAS adsorption or transport because the solution of a single-rate reaction model is an exponential function. Hence, the summation of multiple exponential functions is equivalent to a truncated power-law function. In this study, the truncated power-law late-time tail can be seen in the measured PFAS BTCs shown for full dataset 5 (Fig. 5) and part of dataset 6 (Fig. 6a) and dataset 7 (Figs. 7 and S3), implying multi-rate kinetics for PFAS in most experiments. The short, exponentially declining late-time BTC tail is also observed for part of dataset 6 (Fig. 6b), showing the possibility of several rates or one rate for PFAS transport likely due to weak geochemical heterogeneity and/or experiment limitations (including the detection limit and the relatively short experimental time) in column experiments. Most of the observed PFAS adsorption kinetic curves also evolve as a power-law function in time before reaching stability (Figs. 3 and 4), implying a power-law distribution of adsorption rates. Therefore, the late-time tail of a PFAS BTC can be as extensive as a power-law function, as minimal as an exponential function, or any state transitioning from the power-law to the exponential function.

The assumption that the PDF of PFAS adsorption rate follows the TOSD function (which is called the tempered stable law in this study) was motivated by Cvetkovic (2011) and Meerschaert et al. (2008), who found that the TOSD (defined by Eq. (15)) can be the universal density for hydrologic processes. For example, when the TOSD function (15) is used to define the memory function in PFAS transport, the resultant late-time BTC declines as a power-law function at time $t \ll 1/\lambda$ (due to the power-law distributed mass exchange rate defined by the TOSD function (15)) and then transfers to exponential at time $t \gg 1/\lambda$

(meaning that the transport time is larger than the reciprocal of the smallest mass exchange rate corresponding to the slowest adsorption rate). By adjusting the truncation parameter λ in the TOSD function (15), we can capture PFAS BTCs with any tailing behavior transitioning from power-law to exponential functions.

5.2 TOSD Model Parameters Related to PFAS Chain Length and Soil Properties

The parameters of the TOSD models can be interpreted qualitatively with respect to physicochemical factors controlling PFAS adsorption and mobility in soil. The index α captures the power-law slope of the adsorption rate distribution or the mass exchange rate distribution. A smaller α describes slower adsorption kinetics or a stronger mass exchange during transport. Model applications in sections 2.3, 3.3, and 4.3 show that the time index α in the TOSD models is slightly more sensitive to the soil type than the PFAS type for the data evaluated. This difference implies that the soil properties may cause more variation in the PDF of adsorption rate for PFAS than the PFAS type for the data sets tested herein. The moderate impact of PFAS may be because all 5 PFAS in Fig. 3 are anionic. Greater differences may be exhibited for a wider range of PFAS structures (e.g., cationic, nonionic, zwitterionic). This needs additional testing. The index α also decreases for the column materials with stronger adsorption (Fig. 6a vs. Fig. 6b), as expected (since a smaller α represents more delayed transport and a more extensive elution tail in the PFAS BTC). Notably, for adsorption isotherms, the index α generally decreases with an increasing PFAS chain length (because adsorption is stronger for a longer PFAS chain) (see Fig. 1 and Table 1), implying that α is sensitive to the PFAS type in adsorption isotherms.

The truncation parameter λ in the TOSD adsorption models controls the transition from power-law adsorption to exponential adsorption of PFAS, due to the minimum (i.e., slowest) rate in adsorption or the maximum adsorption capacity. Therefore, the truncation parameter captures the time to achieve the equilibrium state of adsorption for PFAS in soil.

The capacity coefficient β in the TOSD-transport model (21) accounts for the fraction of non-moving mass at equilibrium, which is the combination of the adsorbed mass on the solid phase and the aqueous and solid mass retained in stagnant zones. Therefore, β can capture the co-effect of adsorption and medium heterogeneity on the mobility of PFAS in soil.

The rate constant k in the TOSD-isotherm model (6) scales the isotherm curve plotted in Fig. 1, which increases with increasing PFAS chain length (Table 1). This is functionally similar to the equilibrium concentration C_e in the TOSD-kinetic model (18) (or S_e in model (17)).

5.3 Model Comparison

Adsorption isotherms (Figs. 1 and 2): The TOSD-isotherm model (6) captures the overall pattern of $C_S \sim C_W$ slightly better than the classical Freundlich model (1), especially for the large aqueous and solid phase concentrations of PFAS whose relationship is no longer the power-law function (Fig. 1). In addition, the application shown in Fig. 2 indicates that model (6) can capture a wider range of PFAS adsorption isotherms than the Freundlich model (1). Model (6) is also slightly better than the Langmuir model (2) in fitting the correlation between the large aqueous phase and solid phase concentrations of PFOS, where the solid

phase concentration no longer increases as a power-law function (but rather follows an exponential function) with the increase in the aqueous phase concentration (Fig. 2). Notably, the general model (6) contains one more parameter than the classical isotherm models (1) and (2).

Adsorption kinetics (Figs. 3 and 4): The TOSD-kinetic model (17) can capture any number of adsorption rates and therefore is more general. The biexponential adsorption model (8) fits well the observed adsorption kinetics (Figs. 3 and 4) but has two limitations. First, it contains two more fitting parameters than the TOSD-kinetic model (17). Second, more complex adsorption kinetics (such as adsorption of PFAS in media with stronger geochemical heterogeneity) may require more than two adsorption rates, where the two-rate model (8) is no longer valid, but the TOSD-kinetic model (17) may still be applicable because it captures any number of adsorption rates.

Solute transport (Figs. 5~8): The two-site model (19) and the MIM model (S4) cannot capture the late-time extensive tails of the PFOS BTC observed for Eustis and Vinton soil (Fig. 5 and Fig. S1), or observed for PFOA in the crushed limestone (Fig. 6a and Fig. S2a). This is because both the two-site model (19) and the MIM model (S4) apply an exponential memory function to capture the adsorption processes of PFAS in soil. In addition, although both the TOSD-transport model (21), the two-site model (19), and the MIM model (S4) can capture most of the measured PFOA and PFOS BTCs in an arithmetic plot (Figs. 7a~7d and Figs. S3a~S3d), the TOSD-transport model (21) fits better the late-time BTC tailing clearly shown in a semi-log plot (Figs. 7e~7h and Figs. S3e~S3h).

Inspection of Fig. 5 and Fig. S1 shows that both the TOSD-transport model (21) and the CDMR model (S1) can simulate the observed transport behavior of PFAS in the various soils, including representation of the extensive late-time tailing. The CDMR model (S1) focuses on capturing the adsorption effects on the transport of PFOS in soil and represents the multi-rate adsorption kinetic process by assuming an \ln (natural logarithm)-normal distribution for the distribution of adsorption/desorption kinetic coefficients. Compared to the CDMR model (S1) consisting of three equations, the TOSD-transport model (21) requires only one equation to account for any number of adsorption/desorption rates. The physical interpretation behind PFAS adsorption and mobility is consistent: multi-rate adsorption whose rate distribution can be efficiently captured by the TOSD function. This universal PDF leads to physical models that can generalize the previous models in quantifying a broad range of PFAS adsorption kinetics and transport dynamics in soil.

Other solute-transport models have been proposed that can simulate nonideal behavior such as late-time tailing, including the MRMT and CTRW models discussed in the Introduction. A comparison of the performance, advantages, and disadvantages of the MRMT, CTRW, and CDMR models compared to the TOSD model proposed in this study in quantifying PFAS transport is presented in section S.5 in the SI. It was shown that all four models produce similarly good simulations of the PFAS transport data (Fig. S5 and S6). However, as discussed in the SI, the TOSD model has certain advantages overall, including greater generality, as discussed in the following section.

5.4 Adaptability of the TOSD Models

The TOSD models proposed above were evaluated in the previous sections by comparison to published PFAS data. Here we discuss the adaptability and flexibility of the TOSD models. First, anomalous transport (characterized by a broad range of tailing, truncation, or transition between non-Fickian and Fickian transport) was found to be ubiquitous by several researchers for pollutant transport in various soil and sand columns (e.g., Brusseau and Rao, 1989; Cortis and Berkowitz, 2004; Berkowitz et al., 2006; Meerschaert et al., 2008; Yang and Wang, 2019). As shown by Fig. S4, these transport behaviors (far broader than those observed in the data reviewed above) can be efficiently described by the TOSD-transport model (21) by adjusting the time index (α) (between 1 to 0, to capture the BTC slope), capacity coefficient (β) (to shift vertically the BTC tail), and truncation parameter (λ) (to capture the temporal transition of solute transport dynamics, or from sub-diffusion to normal diffusion).

Second, laboratory column experiments generally represent simplified systems compared to field sites. Transport may be more complex under real-world conditions, requiring extensions of the TOSD models. For example, for a soil column or aquifer with non-stationary heterogeneity, the distributed-order fractional derivative (Chechkin et al., 2002; Yin et al., 2020a) can be adopted in the TOSD-transport model (21):

$$\frac{\partial C_a}{\partial t} + \sum_{i=1}^n \beta_i \frac{\partial^{\alpha_i, \lambda_i} C_a}{\partial t^{\alpha_i, \lambda_i}} - v \frac{\partial C_a}{\partial x} + D \frac{\partial^2 C_a}{\partial x^2}, \quad (22)$$

where the operator $\frac{\partial^{\alpha_i, \lambda_i}}{\partial t^{\alpha_i, \lambda_i}}$ denotes the tempered fractional derivative with the subscript “ i ” denoting the i -th domain characterized by the non-stationary depositional zones. The zone-dependent TOSD-transport model (22) may also be applied to 1) distinguish the contribution of different soil components on adsorption/transport of PFAS, 2) capture bimodal sub-diffusion in strongly heterogeneous porous media (Yin et al., 2020b), and 3) model scale-dependent, asymptotic, non-Fickian transport in heterogeneous porous media due to local, spatial fluctuation of physical/chemical heterogeneity (Zhang et al., 2020).

Third, pollutant transport in aquifers exhibits multiple anomalous features, including direction-dependent spreading rates, channeling along preferential flow paths, trapping of solute in relatively immobile domains, and/or the local variation of transport velocity (e.g., Zhang and Brusseau, 1999; Zhang and Benson, 2008), which can be captured by adding the spatial vector TOSD in the TOSD-transport model (21):

$$\frac{\partial C_a}{\partial t} + \sum_{i=1}^n \beta_i \frac{\partial^{\alpha_i} C_a}{\partial t^{\gamma_i} \lambda_i} - V(t) \frac{\partial C}{\partial x} - \sum_{j=1}^3 \frac{\partial}{\partial x} \left[D_j(x,t) \frac{\partial^{\xi_j-1} C_a}{\partial x^{\xi_j-1} \lambda_j} \right] \quad (23)$$

where ξ_j ($1 < \xi_j < 2$) denotes the index of the tempered fractional derivative in space. Here the TOSD function is extended to space and captures the PDF of velocities along the preferential flow paths. A preliminary test of the vector TOSD-transport model (23) for PFAS transport in the aquifer is shown in section S.6 and Fig. S8 in the SI.

6. CONCLUSION

This study generalized the modeling efforts for the transport and fate of PFAS by proposing and testing a consistent theory (tempered stable law) and general set of models to interpret PFAS dynamics for various types of natural porous media and PFAS. The physical models built upon the TOSD functions captured PFAS sorption and mobility in soil, where the aqueous-phase PFAS concentration exhibited various late-time behaviors, i.e., declining as a power-law function, exponential function, or any intermediate transitional stage. Model comparisons further showed that the three proposed models, including the TOSD-kinetic, -isotherm, and -transport models, fit the observed PFAS concentrations slightly better than the previous models and model parameters were qualitatively related to the physicochemical properties of PFAS in saturated soils exhibiting intrinsic geochemical heterogeneity. This result revealed that both PFAS adsorption kinetics and nonideal transport can be interpreted as a nonequilibrium process dominated by multi-rate adsorption/desorption, where the random adsorption rate follows the tempered one-sided stable PDF. The TOSD function as the PDF for PFAS mass exchange rates (or the tempered stable law) was therefore proposed as the universal law in PFAS adsorption and transport in geomechanics, which requires further experimental and model validation.

Supplementary Material

Refer to Web version on PubMed Central for supplementary material.

ACKNOWLEDGEMENTS

C.M.Z. was supported partially by the National Natural Science Foundation of China (Grant No. 41931292). Y.Z. was funded partially by the University of Alabama CARSCA Program. The contributions of M.L.B. were supported by the NIEHS Superfund Research Program (P42 ES04940). Results of this study do not reflect the views of the funding agencies.

REFERENCES

- Altman D, Machin D, Bryant T, Gardner M, 2013. Statistics with confidence: confidence intervals and statistical guidelines. Second edition, Wiley, ISBN 9781118702505, 1118702506, pp. 256.
- Baeumer B, Haase M, Kovacs M, 2009. Unbounded functional calculus for bounded group with applications. *J. Evol. Equ.* 9, 171–195.
- Berkowitz B, Cortis A, Dentz M, Harvey S, 2006. Modeling non-Fickian transport in geological formations as a continuous time random walk. *Rev. Geophys.* 44(2), 1–49.
- Bromly M, Hinz C, 2004. Non-Fickian transport in homogeneous unsaturated repacked sand. *Water Resour. Res.* 40(7), W07402.
- Brusseau ML, Rao PSC, 1989. Sorption nonideality during organic contaminant transport in porous media. *Crit. Rev. Environ. Control*, 19, 33–99.
- Brusseau ML, 1995. The effect of nonlinear sorption on transformation of contaminants during transport in porous media. *J. Contam. Hydrol.* 17(4), 277–291.
- Brusseau ML, Khan N, Wang Y, Yan N, Van Glubt S, Carroll KC, 2019a. Nonideal Transport and Extended Elution Tailing of PFOS in Soil. *Environ. Sci. Technol.* 53(18), 10654–10664. [PubMed: 31464435]
- Brusseau ML, Yan N, Van Glubt S, Wang Y, Chen W, Lyu Y, Dungan B, Carroll KC, Holguin FO, 2019b. Comprehensive retention model for PFAS transport in subsurface systems. *Water Res.* 148, 41–50. [PubMed: 30343197]
- Brusseau ML, 2020. Simulating PFAS transport influenced by rate-limited multi-process retention. *Water Res.* 168, 115179. [PubMed: 31639593]
- Buck RC, Franklin J, Berger U, Conder JM, Cousins IT, de Voogt P, Jensen AA, Kannan K, Mabury SA, van Leeuwen SP, 2011. Perfluoroalkyl and polyfluoroalkyl substances in the environment: Terminology, classification, and origins. *Integr. Environ. Assess. Manag.* 7, 513–541. [PubMed: 21793199]
- Cao FM; Wang L; Tian Y; Wu FC; Deng CB; Guo QW; Sun HW; Lu SY, 2017. Synthesis and evaluation of molecularly imprinted polymers with binary functional monomers for the selective removal of perfluorooctanesulfonic acid and perfluorooctanoic acid. *J Chromatogr A.* 1516, 42–53. [PubMed: 28823786]
- Chechkin AV, Gorenflo R, Sokolov IM, 2002. Retarding subdiffusion and accelerating superdiffusion governed by distributed-order fractional diffusion equations. *Phys. Rev. E* 66, 046129.
- Chen HT, Reinhard M, Nguyen VT, Gin KYH, 2016. Reversible and irreversible sorption of perfluorinated compounds (PFCs) by sediments of an urban reservoir. *Chemosphere* 144, 1747–1753. [PubMed: 26521093]
- Chen YC, Lo SL, Li NH, Lee YC, Kuo J, 2013. Sorption of perfluoroalkyl substances (PFASs) onto wetland soils. *Desalin. Water. Treat.* 51(40-42), 7469–7475.
- Cortis A, Berkowitz B, 2004. Anomalous transport in “classical” soil and sand columns. *Soil Sci. Soc. Am. J.* 68 (5), 1539–1548.
- Cvetkovic V, 2011. The tempered one-sided stable density: A universal model for hydrological transport? *Environ. Res. Lett.* 6, 034008.
- Foo KY, Hameed BH, 2010. Insights into the modeling of adsorption isotherm systems. *Chem. Eng. J.* 156(1), 2–10.
- Guelfo JL, Wunsch A, McCray J, Stults JF, Higgins CP, 2020. Subsurface transport potential of perfluoroalkyl acids (PFAAs): Column experiments and modeling. *J. Contam. Hydrol.* 103661. [PubMed: 32535327]
- Haggerty R, McKenna SA, Meigs LC, 2000. On the late-time behaviour of tracer breakthrough curves. *Water Resour. Res.* 36, 3467–3479.
- Higgins CP, Luthy RG, 2006. Sorption of perfluorinated surfactants on sediments. *Environ. Sci. Technol.* 40(23), 7251–7256. [PubMed: 17180974]
- Ho YS, Ng JCY, McKay G, 2000. Kinetics of pollutant sorption by biosorbents: Review. *Separ. Purif. Method* 29(2), 189–232.

- Jian J, Guo Y, Zeng L, Liang-Ying L, Lu X, Wang F, Zeng EY, 2017. Global distribution of perfluorochemicals (PFCs) in potential human exposure source—a review. *Environ. Int.* 108, 51–62. [PubMed: 28800414]
- Kucharzyk KH, Darlington R, Benotti M, Deeb R, Hawley E, 2017. Novel treatment technologies for PFAS compounds: A critical review. *J. Environ. Manage.* 204, 757–764. [PubMed: 28818342]
- Lagergren S, 1898. *Kungliga Svenska Vetenskapsakademiens. Handlingar*, Band 24, 1.
- Li F, Fang XL, Zhou ZM, Liao XB, Zou J, Yuan BL, Sun WJ, 2019. Adsorption of perfluorinated acids onto soils: Kinetics, isotherms, and influences of soil properties. *Sci. Total Environ.* 649, 504–514. [PubMed: 30176462]
- Limousin G, Gaudet JP, Charlet L, Szenknect S, Barthes V, Krimissa M, 2007. Sorption isotherms: A review on physical bases, modeling and measurement. *Appl. Geochem.* 22, 249–275.
- Liu LF, Li DY, Li CL, Ji R, Tian XF, 2018. Metal nanoparticles by doping carbon nanotubes improved the sorption of perfluorooctanoic acid. *J. Hazard. Mater.* 351, 206–214. [PubMed: 29550554]
- Lu BQ, Zhang Y, Zheng CM, Green CT, O'Neill C, Sun HG, Qian JZ, 2018. Comparison of time nonlocal transport modes for characterizing non-Fickian transport: From mathematical interpretation to laboratory application. *Water* 10(6), 778.
- Lv X, Sun Y, Ji R, Gao B, Wu JC, Lu QS, Jiang H, 2018. Physicochemical factors controlling the retention and transport of perfluorooctanoic acid (PFOA) in saturated sand and limestone porous media. *Water Res.* 141, 251–258. [PubMed: 29800833]
- Lyu Y, Brusseau ML, Chen W, Yan N, Fu XR, Lin XY, 2018. Adsorption of PFOA at the air–Water interface during transport in unsaturated porous media. *Environ. Sci. Technol.* 52(14), 7745–7753. [PubMed: 29944343]
- Meerschaert MM, Tadjeran C, 2004. Finite difference approximations for fractional advection–dispersion flow equations. *J. Comput. Appl. Math.* 172(1), 65–77.
- Meerschaert MM, Zhang Y, Baeumer B, 2008. Tempered anomalous diffusion in heterogeneous systems. *Geophys. Res. Lett.* 35(17), L17403.
- Miao Y, Guo XT, Peng D, Fan TY, Yang C, 2017. Rates and equilibria of perfluorooctanoate (PFOA) sorption on soils from different regions of China. *Ecotox. Environ. Safe.* 139, 102–108.
- Milinic J, Lacorte S, Vidal M, Rigol A, 2015. Sorption behaviour of perfluoroalkyl substances in soils. *Sci. Total Environ.* 511, 63–71. [PubMed: 25531590]
- Miller KS, Ross B, 1993. *An Introduction to Fractional Calculus and Fractional Differential Equations.* John Wiley, Hoboken, N. J.
- Plazinski W, Rudzinski W, Plazinska A, 2009. Theoretical models of sorption kinetics including a surface reaction mechanism: A review. *Adv. Colloid Interfac.* 152(1-2), 2–13.
- Qiu H, Lv LV, Pan BC, Zhang QJ, Zhang WM, Zhang QX, 2009. Critical review in adsorption kinetic models. *J. Zhejiang Uni. SCIENCE A* 10(5), 716–724.
- Rappazzo KM, Coffman E, Hines EP, 2017. Exposure to perfluorinated alkyl substances and health outcomes in children: a systematic review of the epidemiologic literature. *Int. J. Environ. Res. Public Health.* 14, 691.
- Schumer R, Benson DA, Meerschaert MM, Baeumer B, 2003. Fractal mobile/immobile solute transport. *Water Resour. Res.* 39(10), 1296, doi:10.1029/2003WR002141.
- Shin HM, Vieira VM, Ryan PB, Detwiler R, Sanders B, Steenland K, Bartell SM, 2011. Environmental fate and transport modeling for perfluorooctanoic acid emitted from the Washington works facility in West Virginia. *Environ. Sci. Technol.* 45(4), 1435–1442. [PubMed: 21226527]
- Sun HG, Zhang Y, Chen W, Reeves DM, 2014. Use of a variable-index fractional-derivative model to capture transient dispersion in heterogeneous media. *J. Contam. Hydrol.* 157, 47–58. [PubMed: 24299661]
- United States Environmental Protection Agency (USEPA), 2019. EPA's Per- and Polyfluoroalkyl Substances (PFAS) Action Plan, EPA823R18004, pp. 72. https://www.epa.gov/sites/production/files/2019-02/documents/pfas_action_plan_021319_508compliant_1.pdf
- Weber AK, Barber LB, LeBlanc DR, Sunderland EM, Vecitis CD, 2017. Geochemical and hydrologic factors controlling subsurface transport of poly- and perfluoroalkyl substances, Cape Cod, Massachusetts. *Environ. Sci. Technol.* 51, 4269–4279. [PubMed: 28285525]

- Wei C, Song X, Wang Q, Hu ZH, 2017. Sorption kinetics, isotherms and mechanisms of PFOS on soils with different physicochemical properties. *Ecotox. Environ. Safe.* 142, 40–50.
- Xu C, Chen H, Jiang F, 2015. Adsorption of perfluorooctane sulfonate (PFOS) and perfluorooctanoate (PFOA) on polyaniline nanotubes. *Colloids Surf. A: Physicochem. Eng. Asp.* 479, 60–67.
- Yang XR, Wang Y, 2019. Ubiquity of anomalous transport in porous media: Numerical evidence, continuous time random walk modelling, and hydrodynamic interpretation. *Sci. Rep.* 9, 4601. [PubMed: 30872610]
- Yin MS, Zhang Y, Ma R, Tick GR, Bianchi M, Zheng CM, Wei W, Wei S, Liu XT, 2020a. Superdiffusion affected by hydrofacies mean length and source geometry in alluvial settings. *J. Hydrol.* 582, 124515.
- Yin MS, Ma R, Zhang Y, Wei S, Tick GR, Wang JQ, Sun ZY, Sun HG, Zheng CM, 2020b. A distributed-order time fractional derivative model for simulating bimodal sub-diffusion in heterogeneous media. *J. Hydrol.* 591, 125504.
- Zhang ZH, Brusseau ML, 1999. Nonideal transport of reactive solutes in heterogeneous porous media 5. Simulating regional-scale behavior of a trichloroethene plume during pump-and-treat remediation. *Water Resour. Res.* 35, 2921–2935.
- Zhang CJ, Yan H, Li F, Hu X, Zhou Q, 2013. Sorption of short-and long-chain perfluoroalkyl surfactants on sewage sludges. *J. Hazard. Mater.* 260, 689–699. [PubMed: 23834900]
- Zhang QY, Deng SB, Yu G, Huang J, 2011. Removal of perfluorooctane sulfonate from aqueous solution by crosslinked chitosan beads: sorption kinetics and uptake mechanism. *Bioresour. Technol.* 102(3), 2265–2271.
- Zhang Y, Benson DA, 2008. Lagrangian simulation of multidimensional anomalous transport at the MADE site. *Geophys. Res. Lett.* 35, L07403.
- Zhang Y, Benson DA, Reeves DM, 2009. Time and space nonlocalities underlying fractional-derivative models: Distinction and literature review of field applications. *Adv. Water Resour.* 32(4), 561–581.
- Zhang Y, Zhou DB, Yin MS, Sun HG, Wei W, Li SY, Zheng CM, 2020. Nonlocal transport models for capturing solute transport in one-dimensional sand columns: Model review, applicability, limitations, and improvement. *Hydrol. Process.* 1–19. 10.1002/hyp.13930.
- Zhou HW, Wang CP, Han BB, Duan ZQ, 2011. A creep constitutive model for salt rock based on fractional derivatives. *Int. J. Rock Mech. Min. Sci.* 48(1), 116–121.

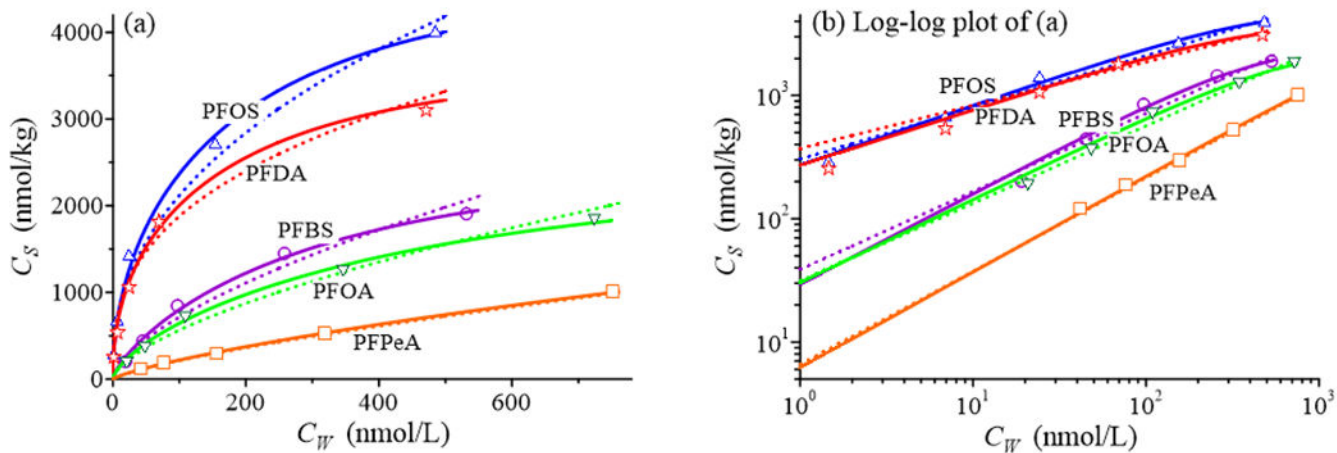


Figure 1. Dataset 1:

sorption isotherms of PFAS onto soil type 6: measured (symbols, from Li et al. (2019)) versus the best-fit (lines) PFAS concentrations. The right plot is the log-log version of the left plot. Each data point represents an average of triplicate data. The dotted and solid lines are calculated using the Freundlich model (1) (according to Li et al. (2019)) and the TOSD-isotherm model (6), respectively.

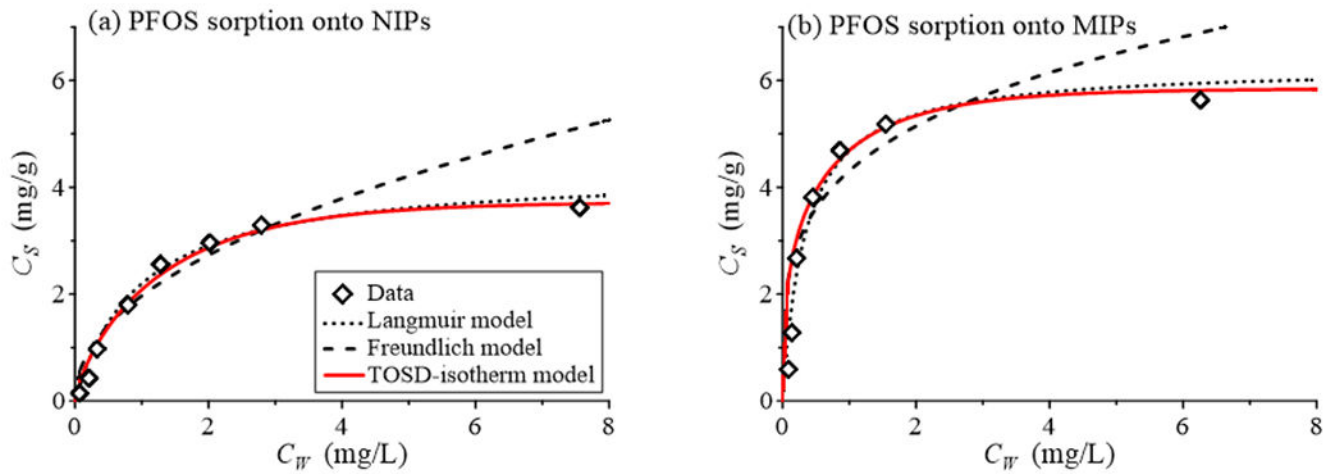


Figure 2. Dataset 2:

sorption isotherms of PFOS onto NIPs (a) and MIPs (b): measured (symbols, from Cao et al. (2017)) versus the best-fit (lines) concentrations of PFOS using the Freundlich model (1), Langmuir model (2) (according to Cao et al. (2017)), and the TOSD-isotherm model (6), respectively.

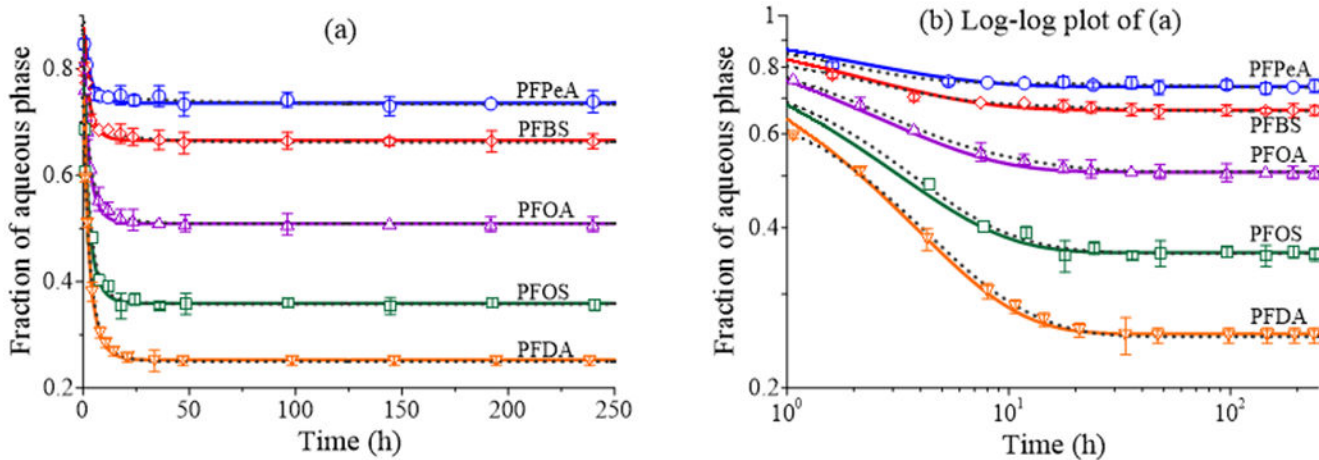


Figure 3. Dataset 3:

Sorption kinetics of different PFAS (five total) onto soil type 1: the observed data (symbols, from Li et al. (2019)) versus the best-fit concentration of the aqueous-phase PFAS using the TOSD-kinetic model (18) (solid lines) and the biexponential adsorption model (8) (dotted lines, by Li et al. (2019)). The right plot is the log-log version of the left plot, to show the early-time tail. The vertical bar for each data represents the standard deviation of triplicate samples.

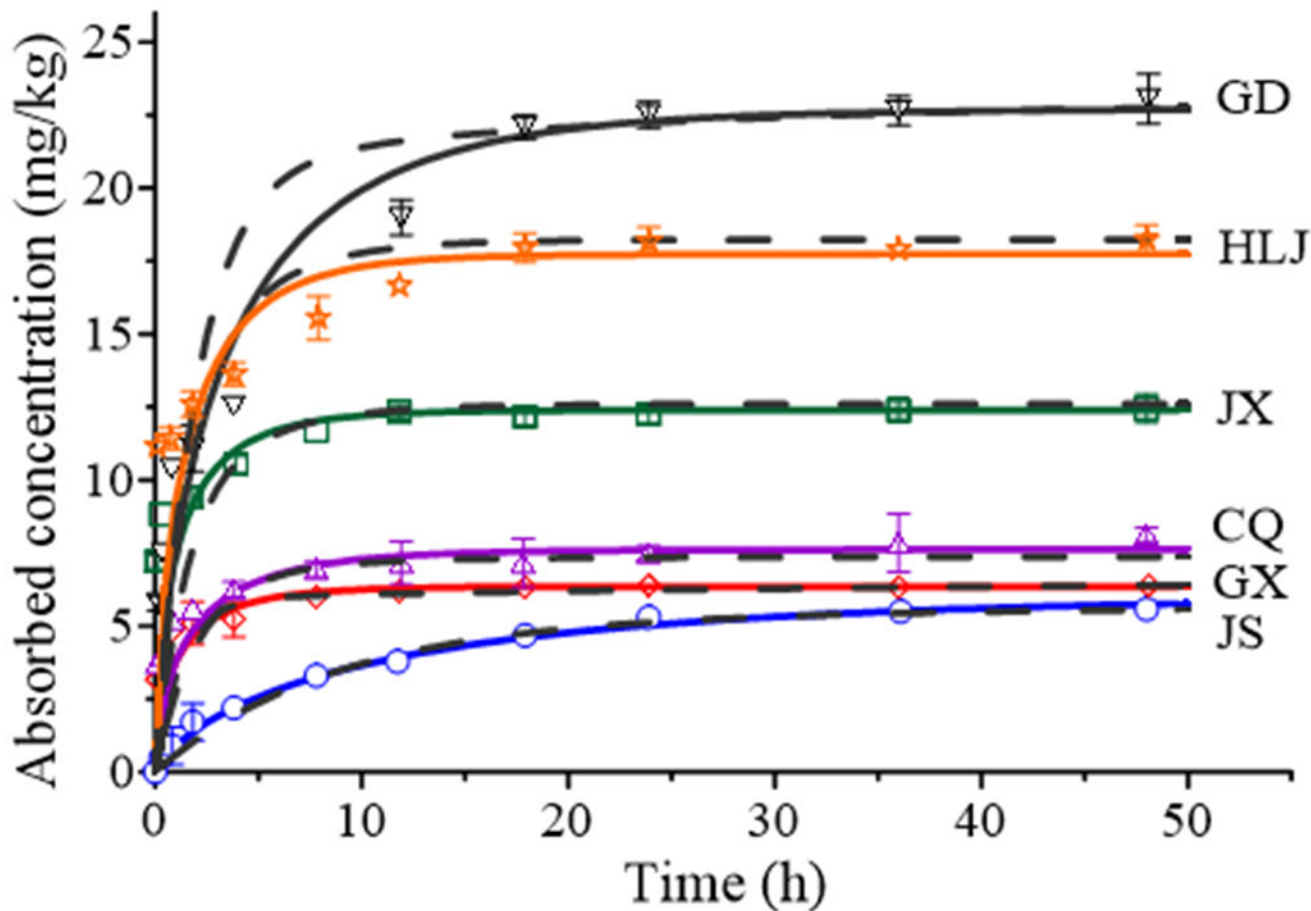


Figure 4. Dataset 4:

Sorption kinetics of PFOS onto different types of soil (six total): the measured (symbols, from Wei et al. (2017)) versus the model solutions for adsorption process (concentration of the absorbed PFAS) using the TOSD-kinetic model (17) (solid lines) and the biexponential adsorption model (8) (dashed lines) fitted by Wei et al. (2017). The vertical bar for each data represents the standard deviation of triplicate samples.

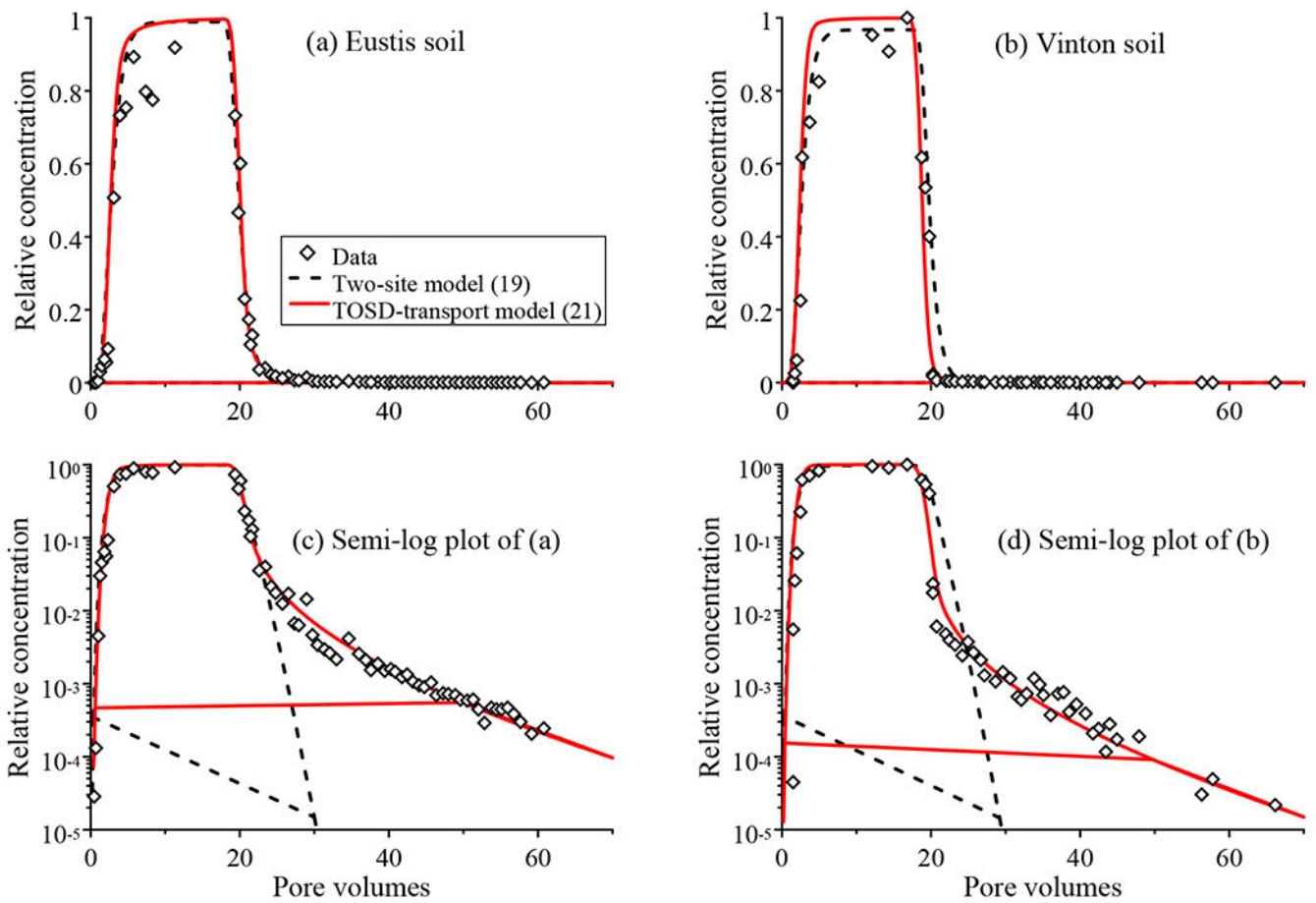


Figure 5. Dataset 5:

Measured (symbols) versus simulated (lines) breakthrough curves for PFOS (Experiment 2, Brusseau et al. (2019)) transport in the Eustis soil (a) and Vinton soil (b). The lines are the best-fit solutions using the two-site model (19) and the TOSD-transport model (21), respectively. (c) and (d) are the semi-log plots of (a) and (b), respectively, to show the late-time tail.

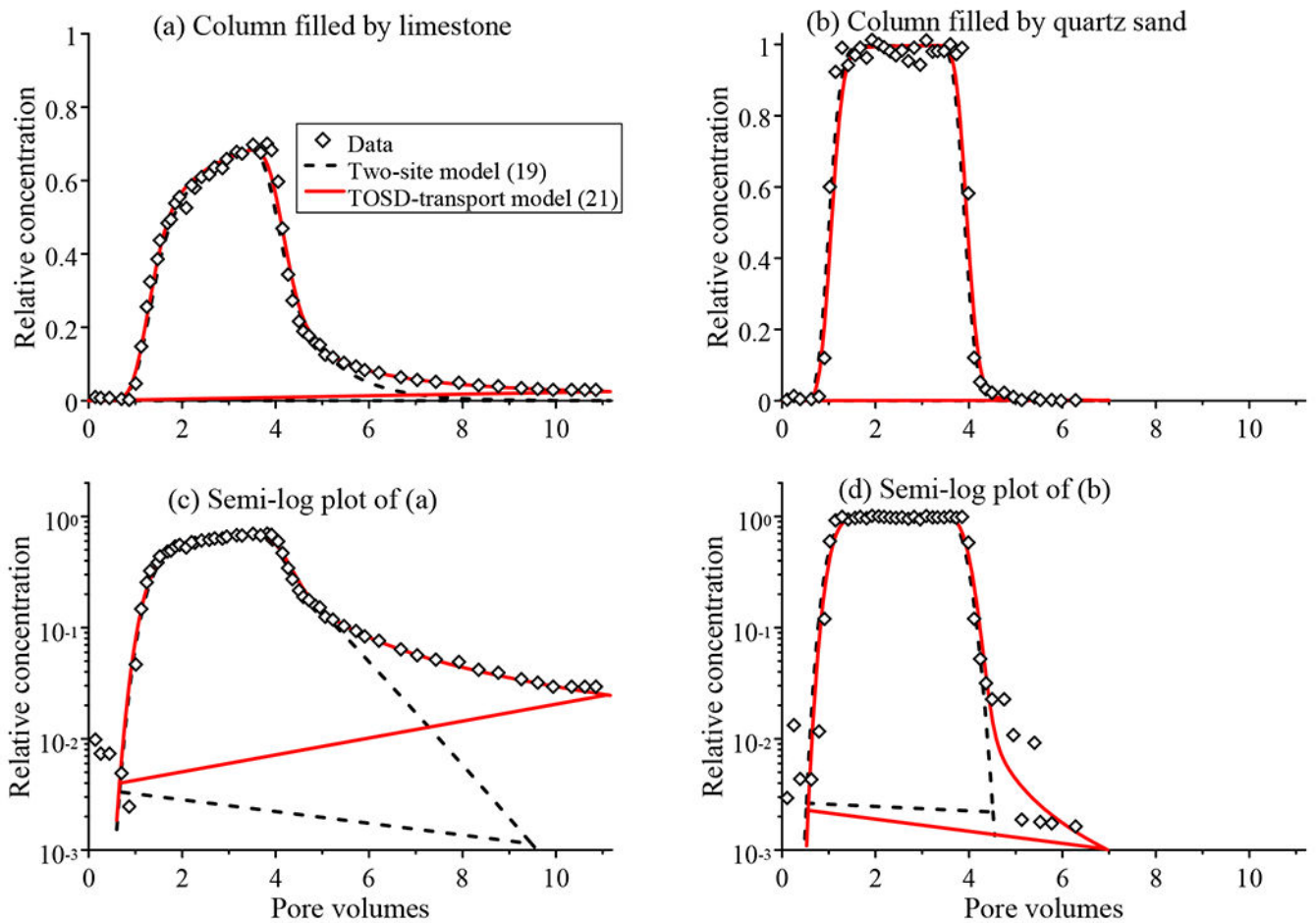


Figure 6. Dataset 6:

Measured (symbols) versus simulated (lines) BTCs for PFOA transport in the column packed with crushed limestone (a) and treated quartz sand (b) (data from Lv et al. (2018)). (c) and (d) are the semi-log plots of (a) and (b), respectively, to show the late-time tail. The lines are the best-fit solutions using the TOSD-transport model (21) and the two-site retention model (19) in Lv et al. (2018), respectively.

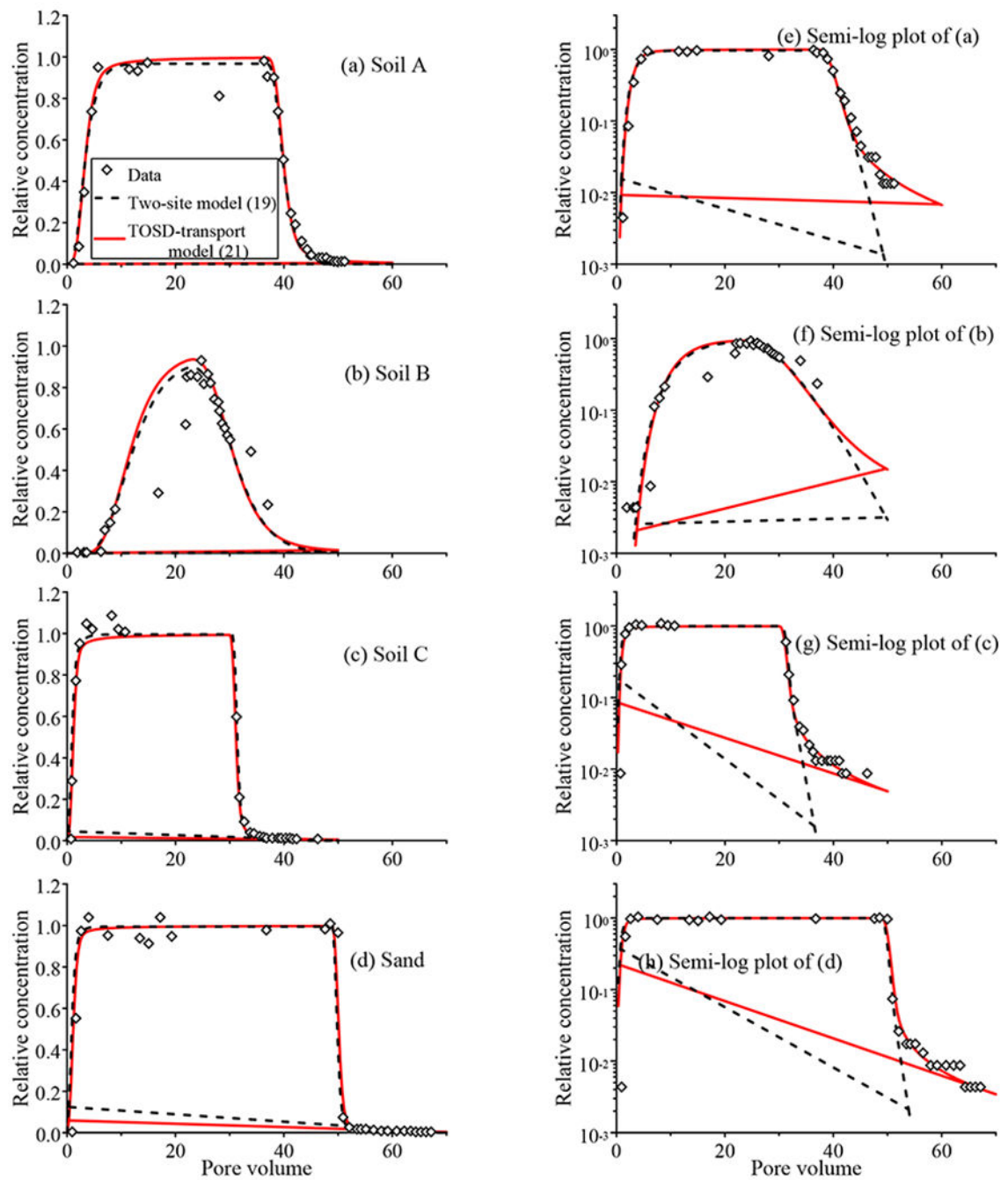


Figure 7. Dataset 7:

Measured (symbols) versus simulated (lines) BTCs for PFOS transport in the column packed with Soil A (a), Soil B (b), Soil C (c), and Sand (d), respectively (data from Guelfo et al. (2020)). The right figure is the semi-log plot of the left figure, to show the late time tail. The lines are the best-fit solutions using the TOSD-transport model (21) and the two-site model (19), respectively.

Table 1.**Dataset 1:**

Best-fit parameters of the TOSD-isotherm model (6) in capturing the adsorption isotherm experiments of various PFAS in Li et al. (2019). In the legend, “ R^2 ” ($0 < R^2 \leq 1$) denotes the coefficient of determination (a larger R^2 represents a better fit), and “(-)” denotes dimensionless.

Perfluorinated acids	TOSD-isotherm model (7)				Freundlich model (1)		
	k ($\text{nmol}^{1-\alpha}\text{L}^{\alpha}\text{Kg}^{-1}$)	α (-)	λ (nmol^{-1}L)	R^2 (-)	k_F ($\text{nmol}^{1-n}\text{L}^n\text{Kg}^{-1}$)	n (-)	R^2 (-)
PFPeA	5.724	0.777	0.0002	0.996	6.574	0.757	0.996
PFBS	26.773	0.740	0.0023	0.996	38.699	0.633	0.972
PFOA	27.397	0.676	0.0014	0.995	31.311	0.628	0.984
PFOS	240.270	0.487	0.0024	0.989	302.482	0.423	0.976
PFDA	240.824	0.450	0.0025	0.990	386.812	0.353	0.972

Table 2.**Dataset 2:**

Summary of parameters of the TOSD-isotherm model (6) in fitting the adsorption isotherm experiments in Cao et al. (2017).

Perfluorinated acids	TOSD-isotherm model (7)				Freundlich model (1)		
	k ($\text{nmol}^{1-\alpha}\text{L}^{\alpha}\text{Kg}^{-1}$)	α (-)	λ (nmol^{-1}L)	R^2 (-)	k_F ($\text{nmol}^{1-n}\text{L}^n\text{Kg}^{-1}$)	n (-)	R^2 (-)
NIPs	2.386	0.742	0.550	0.997	1.970	0.472	0.846
MIPs	4.761	0.342	0.551	0.980	4.310	0.256	0.711

Table 3.**Dataset 3:**

Summary of parameters of the TOSD-kinetic model (18) in fitting the adsorption kinetic experiments for various PFASs in Li et al. (2019).

Perfluorinated acids	C_e (-)	C_0 (-)	α (-)	λ (h ⁻¹)	R^2 (-)
PFPeA	0.738	1	0.280	0.168	0.974
PFBS	0.662	1	0.278	0.174	0.983
PFOA	0.538	1	0.270	0.153	0.992
PFOS	0.358	1	0.252	0.159	0.997
PFDA	0.250	1	0.250	0.158	0.998

Author Manuscript

Author Manuscript

Author Manuscript

Author Manuscript

Table 4.**Dataset 4:**

Summary of parameters of the TOSD-kinetic model (17) in fitting the PFOS adsorption kinetic experiments from Wei et al. (2017).

Soils	S_e (mgkg^{-1})	α (-)	λ (h^{-1})	R^2 (-)
JS	5.77	0.045	0.037	0.998
GX	6.60	0.345	0.209	0.992
CQ	6.77	0.160	0.103	0.981
JX	12.60	0.360	0.208	0.979
HLJ	18.30	0.180	0.095	0.975
GD	22.97	0.130	0.115	0.979

Author Manuscript

Author Manuscript

Author Manuscript

Author Manuscript

Dataset 5:

Table 5.

Summary of parameters of the TOSD-transport model (21) and the two-site model (19) in fitting PFOS transport in soil for **dataset 5** shown in Fig. 5 (Brusseau et al., 2019). In the legend, the symbol “(-)” denotes dimensionless, “RMSE” denotes the root mean square error, and the symbol “±” denotes the 90% confidence interval.

soils	TOSD-transport model (21)					Two-site model (19)						
	D (cm ² /h)	ν (cm/h)	α (-)	β (h ^{α} -1)	λ (h ⁻¹)	RMSE	D (cm ² /h)	ν (cm/h)	k_1 (h ⁻¹)	k_2 (h ⁻¹)	k_3 (h ⁻¹)	RMSE
Vinton soil	0.630	11.66	0.95±0.02	0.52±0.02	0.047	0.071	0.630	11.66	0.006	0.010	0.400	0.127
Eustis soil	0.450	11.21	0.85±0.01	0.62±0.02	0.046	0.066	0.450	11.21	0.006	0.100	0.500	0.114

Dataset 6:

Table 6.

Summary of parameters of the TOSD-transport model (21) and the two-site model (19) in fitting PFOA transport in quartz sand and limestone for **dataset 6** shown in Fig. 6 (Lv et al., 2018). The legends are the same as those used in Table 5.

soils	TOSD-transport model (21)						Two-site model (19)					
	D (cm ² /h)	ν (cm/h)	α (-)	β (h ^{α} -1)	λ (h ⁻¹)	RMSE	D (cm ² /h)	ν (cm/h)	k_1 (h ⁻¹)	k_2 (h ⁻¹)	k_3 (h ⁻¹)	RMSE
Quartz sand	0.294	12.24	0.94±0.02	0.10±0.01	1.00×10 ⁻⁴	0.068	0.294	12.24	3.82×10 ⁻³	1.02×10 ⁻⁴	0	0.079
Limestone	0.366	10.62	0.25±0.01	0.60±0.22	2.00×10 ⁻³	0.025	0.366	10.62	2.34×10 ⁻¹	4.56×10 ⁻¹	1.34	0.042

Dataset 7:

Summary of parameters of the TOSD-transport model (21) and the two-site model (19) in fitting PFOS transport in Soils/Sand for **dataset 7** shown in Fig. 7 (Guelfo et al., 2020). The legends are the same as those used in Table 5.

Table 7.

Soil type	TOSD-transport model (21)					Two-site model (19)						
	D (cm ² /h)	ν (cm/h)	α (-)	β (h ^{0.4} -1)	λ (h ⁻¹)	RMSE	D (cm ² /h)	ν (cm/h)	k_1 (h ⁻¹)	k_2 (h ⁻¹)	k_3 (h ⁻¹)	RMSE
Soil A	0.011	0.08	0.82±0.02	0.40±0.01	1.00×10 ⁻²	0.140	0.011	0.08	0.0184	0.278	0.90	0.131
Soil B	0.003	0.02	0.70±0.02	0.40±0.02	1.00×10 ⁻²	0.271	0.003	0.02	0.0115	0.201	0.91	0.280
Soil C	0.003	0.15	0.75±0.01	0.40±0.02	1.00×10 ⁻⁴	0.140	0.003	0.15	0.0058	0.104	0.92	0.143
Sand	0.005	0.26	0.81±0.02	0.40±0.02	1.00×10 ⁻⁴	0.134	0.005	0.26	0.0075	0.124	0.98	0.138